ISSN 0015-4628, Fluid Dynamics, 2024, Vol. 59, No. 1, pp. 60–73. © Pleiades Publishing, Ltd., 2024.

The Diffusion Stability of an Externally Driven Cavitation Bubble in Micro-Confinement

K. V. Leonov[a],* and I. Sh. Akhatov[a]

[a] *Bashkir State Medical University, Ufa, Russia*

**e-mail: k.leonoff@inbox.ru*

Received August 3, 2023; revised September 10, 2023; accepted September 21, 2023

Abstract—The diffusion stability of a single cavitation bubble in a spherical liquid cell surrounded by an infinite elastic solid is considered. The time-periodic pressure in the solid far away from the liquid cell is used as an external driving, which initiates bubble oscillations along with the gas diffusion process in the bubble-in-cell system. The work is based on the engineering approximation according to which the bubble growth/reduction is considered on average, assuming that during the period of the external driving the mass of gas in the bubble does not noticeably change. This theory predicts the existence of stably oscillating bubbles in confined liquid undergoing an external driving force. Three possible diffusion regimes are revealed: 1) total bubble dissolution, 2) partial bubble dissolution, and 3) partial bubble growth, where the last two regimes provide the diffusion stability in the bubble-in-cell system. The parametric study of the influence of the gas concentration dissolved in the liquid on the resulting stable bubble size is conducted. The obtained results are compared with the results for the case of the stable bubble oscillations in the pressure sound field in a bulk (infinite) liquid. The theoretical findings of the present study can be used for improvement of the modern applications of ultrasound technology.

Keywords: bubble dynamics, cavitation, ultrasound, diffusion

DOI: 10.1134/S0015462823602413

Bubbles have been studied from many different points of view since their behavior is crucial to a wide variety of applications such as food industry, water treatment, oil extraction, and etc. [1]. Bubbles subject to acoustic waves are associated with applications of liquid degassing by triggering cavitation of gas-containing bubbles [2], and used in many ultrasonic cleaning processes, for instance, in the cleaning of silicon wafers and computer components [3, 4]. Acoustically excited bubbles can disturb local flow field resulting in enhancement of chemical reactions [5] and mixing in microfluidic systems [6]. The use of the high energy ultrasound can induce cavitation effect in extra heavy oil, which can tear large molecules in extra heavy oil into light hydrocarbon molecules reducing the viscosity of the solution and improving transportability [7]. Microbubbles are currently in clinical use as effective ultrasound contrast agents, which consist of a low solubility gas core with a stabilizing shell [8]. Their size allows them free flow through the vasculature, while their gas core provides ultrasound imaging contrast enhancement owing to the mismatch in acoustic impedance between gas and the surrounding blood and soft tissue. Further, the incident ultrasonic field can induce volumetric oscillations of microbubbles, leading to increased scattering and improved image contrast. This effect can be amplified by driving bubbles at their resonance frequency, which typically occurs within the clinically approved frequency range for diagnostic ultrasound. Microbubbles have also been widely studied for their potential to enhance drug delivery for treatment of diseases [8–11]. In combination with ultrasound, they are capable of locally increasing cell membrane permeability to enhance drug uptake – the process is known as sonoporation. Therapeutic payloads can also be directly incorporated into bubbles themselves and their release triggered using high intensity ultrasound, which produces expansion and subsequent collapse of bubbles disrupting a stabilizing shell. The enhanced localized delivery has allowed therapeutic benefit to be observed with lower doses of drugs and hence reduced off-site toxicity.

In the most of the above-mentioned examples the acoustically driven cavitation activity takes place in highly confined spaces. It was shown in the experiments that the gas diffusion across ultrasound-driven microbubbles in the confinement of nano- and micro-channels can (partially) block them and impede their proper use [12]. In this case, bubbles are usually formed either of dissolved gas in the liquid, or liquid

vapor originating from boiling or chemical processes occurring along the channel. It should be mentioned that in the absence of the external sound field, bubbles of any size are unstable because the pressure inside a bubble is larger than in the liquid due to surface tension, and therefore a bubble tends to dissolve slowly. On the other hand, bubble oscillations forced by the periodic acoustic field initiate gas flows in and out of a bubble. This phenomenon is called the rectified diffusion and usually leads to a growth of a bubble [13].

One of the most representative examples of the influence of the rectified diffusion in confined liquid on industrial applications is the inkjet printing technology (see [14] and references therein). In industrial settings the drop-on-demand piezoacoustic inkjet printing is a widespread technological application of microfluidics, which is used in the graphic printing industry. In this technique, a piezoacoustic printhead can jet single droplets on demand out of the nozzle by driving the ink out of the nozzle thanks to deformation of a piezoelectric element and the resulting pressure field. Under certain conditions an air bubble can be entrained in the nozzle, in particular at large jetting frequencies beyond 20 kHz. The bubbles were shown to nucleate on inkophobic dirt particles suspended in the ink. Other potential entrainment mechanisms include the bubble pinch-off from an inward gas jet formed at the oscillating air-ink meniscus driven by flow focusing and the cavitation inception in the rarefaction phase of the pressure wave [15]. Most inks are not pure liquids, but have a very complex composition, containing multiple liquids with different material properties, pigments, other colloidal particles, latex, cross-linkers, surfactants, and polymers, which also increases the probability of bubble nucleation on suspended particles in the ink. After that, the bubble grows by the rectified diffusion, as the ink contains some amount of dissolved gas, resulting in modification of the drop production process and breakdown of the jetting. Once a bubble is entrained, it can practically be flushed out together with the drop within a few actuation cycles or eliminated through diffusive dissolution, i.e., by switching off the piezoactuation for a period of the order of seconds to minutes [16]. These methods consume both ink and time and are therefore highly undesirable. Thus, the bubble entrainment and following rectified diffusion in confined liquid are the significant technological issues in modern industrial digital printing.

The problem of mass transport of gas dissolved in a bulk liquid around a bubble undergoing volume oscillation has been studied extensively [17–22]. Theoretical studies on the rectified diffusion in a microscopic confinement have received little attention so far. Currently, there are several three-layer geometry models of confined bubbles [23–28], which assume a fixed amount of gas in a bubble. In [28] the dynamics of a bubble in a spherical liquid cell entrapped within an infinite elastic solid is studied in the case when the pressure in the solid far away from a bubble is used as a governing dynamic parameter. In this study, the authors did the analysis of the natural bubble oscillations and considered the dynamic response of small and large bubbles in the states below and above the cavitation threshold, respectively. The dynamics of a cavitation bubble in confined liquid has a particular interest in terms of the rectified diffusion, which depends on the bubble volume oscillations. In [29] the authors extended the model developed in [28] and considered the influence of dissolved gas on dynamics of a cavitation bubble in confined liquid. The analysis showed the existence of the regimes of the bubble dynamics, which can provide the formation of a resulting stable bubble. When referring to the stable bubble, the authors mean that the bubble size keeps constant during the volume oscillations on average. In this case, the mass of dissolved gas provides mutual compensation of the mass fluxes in and out of the bubble. In [29] a bubble changes its size starting from the bubble nucleus, which grows/dissolves due to the rectified diffusion. In the present study, the equilibrium diagram of the diffusion stability of the bubble is developed, and an influence of concentration of dissolved gas in confined liquid on the bubble dynamics, which accompanies the formation of the resulting stable bubble, is analyzed. We show that there are the three possible diffusion regimes: 1) total bubble dissolution, 2) partial bubble dissolution, and 3) partial bubble growth, where the last two regimes can be formed under the condition of the three dynamic regimes of the bubble: 1) in the presence of cavitation inception, 2) in the absence of cavitation, and 3) combination of the previous two dynamic regimes.

1. MATHEMATICAL MODEL

1.1. Dynamic Model for a Bubble in a Liquid Cell. The Case of a Fixed Mass of Gas in a Bubble

As a reference, we introduce and further develop the model presented in [29] starting from the concept of the insoluble bubble, where the spherical liquid cell with a bubble inside entrapped within an infinite elastic solid medium, and exposed to tension, or negative pressure as it is shown in Fig. 1. The system of

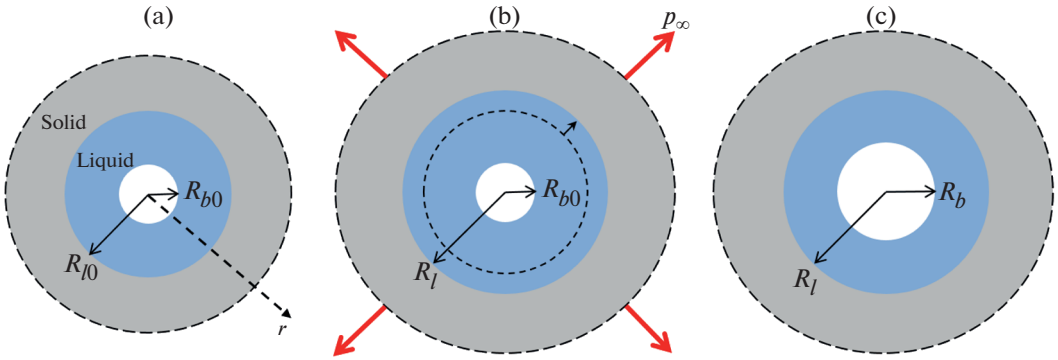

Fig. 1. The configuration of quasi-static states of the system: (a) the reference state, (b) the uniform expansion under tension p_∞, (c) the new equilibrium state.

equations for the dynamics of a confined bubble of constant mass accounting for the pressure far away from the bubble as the driving parameter was derived in [28]:

$$\frac{R_l^3 - R_{l0}^3}{R_{l0}^3} = -\frac{p_\infty(t) - p_0}{K} + \frac{3}{4G}(p_l - p_\infty(t));$$

$$R_b\frac{d^2R_b}{dt^2} + \frac{3}{2}\left(\frac{dR_b}{dt}\right)^2 A_1(R_b, R_l) + \frac{dR_b}{dt}\frac{dR_l}{dt}A_2(R_b, R_l) + \left(\frac{dR_l}{dt}\right)^2 A_3(R_b, R_l) + R_l\frac{d^2R_l}{dt^2}A_4(R_b, R_l) \tag{1.1}$$

$$= \frac{1}{\rho_l \Phi(R_b, R_l)}\left(p_g + p_V(T) - \frac{2\sigma}{R_b} - p_l - 4\mu\frac{\dot{R}_b/R_b - \dot{R}_l/R_l}{1 - \left(\frac{R_b}{R_l}\right)^3}\right),$$

$$\rho_l = \rho_{l0}\frac{R_{l0}^3 - R_{b0}^3}{R_l^3 - R_b^3}, \quad \Phi(R_b, R_l) = \frac{1 - \frac{9}{5}\varepsilon + \varepsilon^3 - \frac{\varepsilon^6}{5}}{(1-\varepsilon^3)^2}, \quad \varepsilon = \frac{R_b}{R_l},$$

$$A_1(R_b, R_l) = \frac{1 + \frac{8}{5}\varepsilon + \frac{2}{5}\varepsilon^2}{(1+\varepsilon+\varepsilon^2)\left(1 + \frac{6}{5}\varepsilon + \frac{3}{5}\varepsilon^2 + \frac{1}{5}\varepsilon^3\right)}, \quad A_2(R_b, R_l) = -\frac{3\varepsilon(2\varepsilon^2 + 8\varepsilon + 5)}{(\varepsilon^2 + \varepsilon + 1)(\varepsilon^3 + 3\varepsilon^2 + 6\varepsilon + 5)},$$

$$A_3(R_b, R_l) = \frac{3\varepsilon^2(2\varepsilon^2 + 8\varepsilon + 5)}{2(\varepsilon^2 + \varepsilon + 1)(\varepsilon^3 + 3\varepsilon^2 + 6\varepsilon + 5)}, \quad A_4(R_b, R_l) = \frac{3}{10}\frac{1 + 3\varepsilon + \varepsilon^2}{1 + \frac{6}{5}\varepsilon + \frac{3}{5}\varepsilon^2 + \frac{1}{5}\varepsilon^3},$$

where R_{b0} and $R_b(t)$ are the reference and current bubble radius, respectively; R_{l0} and $R_l(t)$ are the reference and current liquid cell radius, respectively, $R_{b0} \ll R_{l0}$; ρ_{l0} ($\rho_l(t)$) is the liquid density at the reference (current) state, p_0 is the reference atmospheric pressure, $p_\infty(t)$ is the pressure of the external driving, σ is the surface tension coefficient for the liquid and gas/vapor interface, μ is the dynamic viscosity of the liquid, K and G are the bulk and shear moduli of the elastic solid, respectively. The upper dots denote time derivatives. It is assumed that the bubble contains a fixed amount of a noncondensable and insoluble gas, and saturated vapor of constant pressure $p_V(T)$, corresponding to the fixed system temperature. The pressure range considered in this study is much less than the bulk modulus of the liquid, such that the liquid bulk modulus E_V is assumed to be constant. Thus, the liquid and gas equations of state are as follows:

$$p_l = p_0 - E_V\frac{R_l^3 - R_b^3 - R_{l0}^3 + R_{b0}^3}{R_{l0}^3 - R_{b0}^3}, \quad p_g = \left(p_0 - p_V(T) + \frac{2\sigma}{R_{b0}}\right)\left(\frac{R_{b0}}{R_b}\right)^3.$$

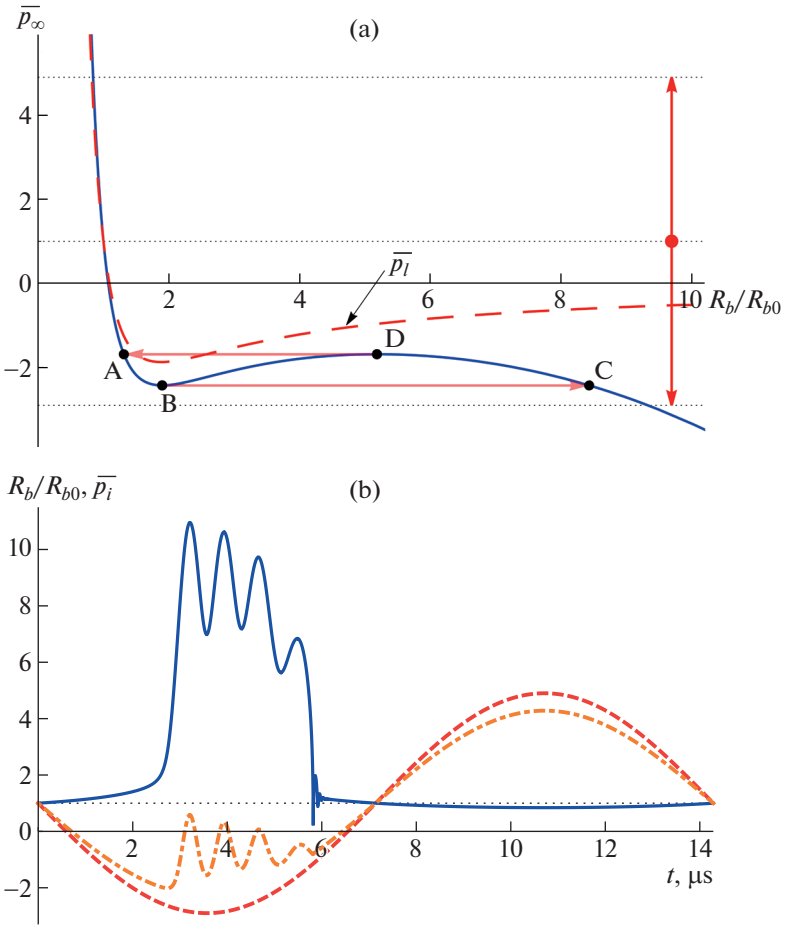

Fig. 2. (a) The dependence of the non-dimensionalized tension in the solid on the bubble radius for $R_{b0} = 272$ nm (or $\overline{\Re_{b0}^{\bullet}} \approx 0.19$ in Fig. 3, full circle). The dotted line $\overline{p_\infty} = 1$ corresponds to the reference state. The dashed line is the liquid pressure $\overline{p_l} = p_l/p_0$. The double arrow illustrates the pressure amplitude of the external driving $\Delta p = 390$ kPa; (b) The evolution of the bubble radius (solid line), the liquid pressure (dot-dashed line), and the external driving (dashed line) at $\Delta p = 390$ kPa, $f_{\text{ext}} = 70$ kHz.

The liquid motion is considered spherically symmetric, and the liquid velocity field in this case has only a radial component v_r [28]:

$$v_r(r,t) = \frac{R_l^3 - r^3}{R_l^3 - R_b^3}\frac{R_b^2\dot{R}_b}{r^2} + \frac{r^3 - R_b^3}{R_l^3 - R_b^3}\frac{R_l^2\dot{R}_l}{r^2}, \tag{1.2}$$

where r denotes the radial distance from the bubble center.

The quasi-static behavior of the bubble-in-cell system can be treated setting all time derivatives in the system of Eqs. (1.1) to zero, which results in the following system

$$\begin{gathered}\frac{R_l^3 - R_{l0}^3}{R_{l0}^3} = -\frac{p_\infty - p_0}{K} + \frac{3}{4G}(p_l - p_\infty);\\ p_l + \frac{2\sigma}{R_b} = p_g + p_V(T),\end{gathered} \tag{1.3}$$

where the first equation is the equation for liquid cell alteration, and the second one is the pressure balance equation for a confined bubble. The solution of the system (1.3) is presented in Fig. 2a as the dependence of tension in the solid $\overline{p_\infty} = p_\infty/p_0$ on the bubble radius. Numerical calculations have been conducted for

$R_{b0} = 272$ nm, $R_{l0} = 40$ μm, $\sigma = 0.07286$ N/m, $\rho_{l0} = 10^3$ kg/m^3, $p_0 = 0.1$ MPa, $p_V = 2338$ Pa, $E_V = 2.2$ GPa, $K = 4.5$ GPa, and $G = 0.74$ GPa for water as a liquid and nitrogen as a gas at $T = 293$ K. The values of the shear modulus G and bulk modulus K of the solid are chosen to correspond to cavitation experiments in a stiff polymer hydrogel [30].

Points A and B in Fig. 2a correspond to stable (below the cavitation threshold) and critical (the cavitation threshold) bubble states, respectively. The critical bubble will grow to a finite size, marked as point C, whereas in the model of a bulk liquid a bubble undergoes an infinite growth (see [31]). The states B–D are unstable. After that, if the tension increases, the bubble will continuously grow, otherwise, the bubble will be continuously compressed down to the radius at metastable point D and will collapse to the radius at point A with the following continuous bubble contraction. In this approach, the bubble contains the fixed mass of gas, which resists total bubble compression.

The nonlinear bubble dynamics is given by the solution of the system of Eqs. (1.1), and shown in Fig. 2b by a solid line along with the pressure in the liquid cell (dot-dashed line), and the periodic external driving in the solid (dashed line), which is given in the form:

$$p_\infty(t) = p_0 - \Delta p \sin(2\pi f_{\text{ext}} t),$$

where $f_{\text{ext}} = 70$ kHz is the driving frequency, $\Delta p = 390$ kPa is the amplitude of pressure oscillations, which provides the cavitation inception and the cavitation vanishing [31], and indicated by the double arrow in Fig. 2a. The dynamic viscosity of water equals $\mu = 10^{-3}$ Pa s for calculations of the bubble dynamics.

1.2. The Incorporation of Gas Diffusion

To incorporate the gas diffusion in this model, the authors assumed that the liquid cell has some amount of dissolved gas, which is involved in the mass transfer across the dynamic interface associated with an oscillating bubble, such that the total amount of gas in the bubble-in-cell system is assumed to be constant and the mass fluxes to an external medium are absent [29]. The formulation of the problem includes the following governing equations:

$$\frac{\partial \tilde{c}}{\partial t} + v_r(r,t)\frac{\partial \tilde{c}}{\partial r} = \frac{D}{r^2}\frac{\partial}{\partial r}\left(r^2 \frac{\partial \tilde{c}}{\partial r}\right), \tag{1.4}$$

$$\tilde{c}\big|_{r=R_b(t)} = H\left(p_0 - p_V(T) + \frac{2\sigma}{R_{b0}}\right)\left(\frac{R_{b0}}{R_b(t)}\right)^3, \tag{1.5}$$

$$\frac{\partial \tilde{c}}{\partial r}\bigg|_{r=R_l(t)} = 0, \tag{1.6}$$

$$\tilde{c}\big|_{t=0} = c_\infty, \tag{1.7}$$

$$\frac{dm_g}{dt} = 4\pi R_b^2(t) D \frac{\partial \tilde{c}}{\partial r}\bigg|_{r=R_b(t)}. \tag{1.8}$$

Here, Eq. (1.4) describes the convective diffusion, where $\tilde{c}$ is the mass concentration of gas dissolved in the liquid cell; $v_r(r,t)$ is the radial velocity field in the liquid cell (see Eq. (1.2)) and D is the diffusivity of gas in the liquid. The Eqs. (1.5) and (1.6) are the boundary conditions at the bubble surface and the surface of the liquid cell, respectively, where H is the Henry's constant. Equation (1.7) is the initial condition, where c_∞ is the uniform gas concentration in the liquid, where the bubble is assumed to be created. Equation (1.8) is the rate of the mass transfer across the bubble interface, where m_g is the mass of gas in the bubble.

This mass transport problem was solved approximately for a large Peclet number ($\text{Pe} = R_{b*}^2 \Omega_* / D \gg 1$), using normalized Lagrangian coordinates to avoid difficulties because of the moving boundary conditions:

$$\eta = \frac{\xi^3 - x^3(\tau)}{\beta(\tau) - (1-\alpha)x^3(\tau)},$$

$$\alpha = \frac{1}{1+\frac{4G}{3E_V}\left(1-\left(\frac{R_{b0}}{R_{l0}}\right)^3\right)}, \quad \beta(\tau) = \left(\frac{R_{l0}}{R_{b*}}\right)^3 - \alpha\left[\left(\frac{R_{b0}}{R_{b*}}\right)^3 + \left(1+\frac{4G}{3K}\right)\frac{R_{l0}^3 - R_{b0}^3}{R_{b*}^3}\frac{p_\infty(\tau)-p_0}{E_V}\right],$$

where $R_{b*} = \frac{2\sigma}{p_0}$ is the typical bubble size in the liquid at ambient pressure p_0 [32]; $\xi = \frac{r}{R_{b*}}$, $x(\tau) = \frac{R_b(\tau)}{R_{b*}}$; $\tau = t\Omega_*$, where Ω_* is the natural frequency of radial oscillations of a bubble with the characteristic radius R_{b*} [28]:

$$\Omega_* = \frac{1}{2\pi R_{b*}}\sqrt{\frac{3}{\rho_{l0}}\left(p_0 - p_V(T) + \frac{4\sigma}{3R_{b*}}\right)}.$$

Following [29] we use the engineering approximation here that the bubble oscillations are fast, and the growth/reduction of the mean bubble size is slow, such that one can split the mass transfer problem into two parts. In the first part, we neglect the effect of the mass transport in the system on the fast bubble oscillations, whereas in the second part we consider the bubble growth/reduction on average, assuming negligible change of the mass of gas in the bubble during the period of the external driving. The latter is characterized by the slow convection-enhanced diffusion and considered in a second timescale $\lambda = \frac{tD}{R_{b*}^2}$, which captures the slow diffusive behavior. In [29] the authors showed that the mass transfer in the bubble-in-cell system consists of the two sequential physically consistent regimes: 1) the growing depletion layer, and 2) the gas diffusion within the liquid cell. Both regimes are characterized by the similar dependency of the time averaged rate of mass transport, which has the form:

$$\frac{dm_g^*}{d\lambda} = \frac{c_\infty - C^*(\lambda)}{T_{\rm rd}}, \tag{1.9}$$

where $m_g^* = \frac{m_g}{m_{\rm liq}^*}$ is the mass of gas in the bubble divided by the mass of the liquid, displaced by the volume of the characteristic bubble, $m_{\rm liq}^* = \rho_{l0}\frac{4\pi R_{b*}^3}{3}$. The function $C^*(\lambda)$ is the averaged gas concentration on the bubble interface:

$$C^*(\lambda) \equiv c_{\rm sb}\left\langle x^{-3}(\tau)\right\rangle_{\hat\tau_1},$$

$$c_{\rm sb} = c_{\rm sp}\left(1+\frac{8}{p_0^*\overline{R_{b0}}{\rm We}}\right)\overline{R_{b0}}^3, \quad p_0^* = \frac{p_0 - p_V(T)}{\frac{1}{2}\rho_{l0}R_{b*}^2\Omega_*^2}, \quad \overline{R_{b0}} = \frac{R_{b0}}{R_{b*}}, \quad {\rm We} = \frac{2\rho_{l0}(R_{b*}\Omega_*)^2 R_{b*}}{\sigma},$$

where $c_{\rm sp} = H^* p_0^*$ is the saturation concentration in the liquid separated from gas at pressure p_0^* by a plane boundary, $H^* = \frac{1}{2}\rho_{l0}R_{b*}^2\Omega_*^2 H$; $c_{\rm sb}$ is the saturation concentration in the liquid separated from gas within a spherical bubble of dimensionless radius $x = 1$; We is the Weber number. The function $T_{\rm rd}$ is the dimensionless characteristic time of the mass growth rate of the bubble ($T_{\rm rd} > 0$), which depends on the regime of the mass transfer. In this approach, two different averaging procedures for the solution of the diffusion problem are used. First, ordinary averaging over the dimensionless period $T_{\rm ext}$ of the acoustic field

$$\left\langle f(\eta,\tau)\right\rangle_\tau = \frac{1}{T_{\rm ext}}\int_0^{T_{\rm ext}} f(\eta,\tau)\,d\tau,$$

which is incorporated in the function $T_{\rm rd}$, and second, a "nonlinear averaging" procedure in a specific nonlinear timescale

$$\left\langle f(\eta,\tau)\right\rangle_{\hat\tau_1} = \frac{1}{\int_0^{T_{\rm ext}}\frac{9x^4(\tau)}{[\beta(\tau)-(1-\alpha)x^3(\tau)]^2}d\tau}\int_0^{T_{\rm ext}} f(\eta,\tau)\frac{9x^4(\tau)}{[\beta(\tau)-(1-\alpha)x^3(\tau)]^2}d\tau.$$

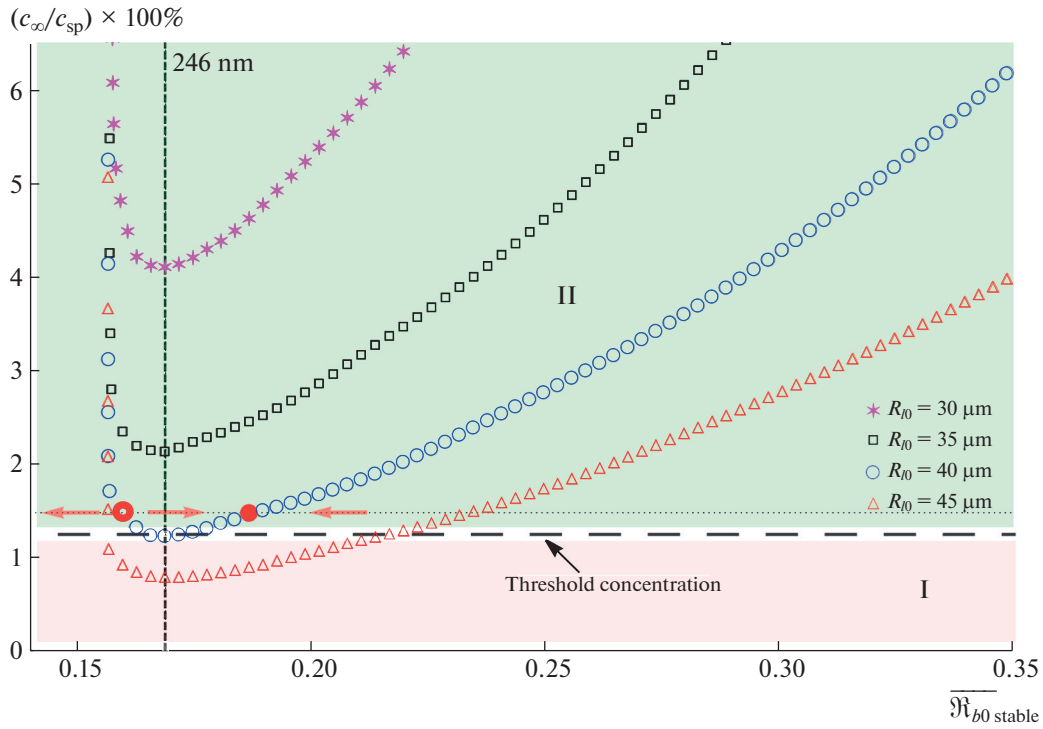

Fig. 3. The dependence of the gas concentration in the liquid cell on the resulting stable bubble size $\overline{\Re_{b0}} = \Re_{b0}/R_{b*}$ for different liquid cell sizes in the range $R_{l0} = 30 \div 45$ μm ($\Delta p = 390$ kPa, $f_{\mathrm{ext}} = 70$ kHz).

In comparison with [29], in the present study we do not consider the evolution of the bubble size during the mass transfer and assume that the bubble nucleus has already reached the resulting stable bubble size $\Re_{b0}$. As a result, the rate of the mass transport (1.9) equals to zero, which allows to consider the equilibrium diagram of the diffusion stability of the bubble (see Fig. 3). The set of physical parameters and the form of the external driving are chosen to be the same as it is introduced above.

2. STABILITY ANALYSIS

As a reference, we consider the case of the liquid cell size $R_{l0} = 40$ μm (open circles in Fig. 3). The total dissolution of the bubble of any size is expected for the gas concentration c_∞ in the range $0 \div 1.24\%$ of c_{sp} (region I in Fig. 3), where during bubble oscillations the mass fluxes out of the bubble exceed the mass fluxes in the bubble on average. The gas concentration 1.25% of c_{sp} is the threshold concentration, which provides the formation of the stable nonzero bubble size $\Re_{b0}^{\mathrm{thres}} = 246$ nm (or $\overline{\Re_{b0}^{\mathrm{thres}}} \approx 0.17$ in Fig. 3). It means that for the fixed gas concentration in the liquid the bubble of any nonzero size changes such that the resulting stable bubble size will be equal $\Re_{b0}^{\mathrm{thres}}$. For the gas concentration c_∞ more than 1.25% of c_{sp} there is the stable state of the bubble, which depends on the certain value of the gas concentration in the liquid (region II in Fig. 3). As an example, we consider the case when the gas concentration c_∞ is 1.48% of c_{sp} (dotted line, Fig. 3). Two values of the bubble radius correspond to this gas concentration: $\Re_{b0}^{\circ} = 233$ nm (or $\overline{\Re_{b0}^{\circ}} \approx 0.16$ in Fig. 3, bold empty circle) and $\Re_{b0}^{\bullet} = 272$ nm (or $\overline{\Re_{b0}^{\bullet}} \approx 0.19$ in Fig. 3, full circle). The radius $\Re_{b0}^{\circ} = 233$ nm is unstable and bubbles with radius $\Re_{b0} < \Re_{b0}^{\circ}$ dissolve due to diffusion flux from the bubble into the liquid. The partial bubble growth is observed for bubbles with radius $\Re_{b0}^{\circ} < \Re_{b0} < \Re_{b0}^{\bullet}$, which grow until they reach the stable radius $\Re_{b0}^{\bullet}$. If the bubble size is larger than $\Re_{b0}^{\bullet}$, the bubble shrinks to the radius $\Re_{b0}^{\bullet}$, i.e., the partial bubble dissolution realizes. Thus, the bubble size $\Re_{b0} > \Re_{b0}^{\circ}$ is the prerequisite condition for the diffusion stability of the bubble in confined liquid.

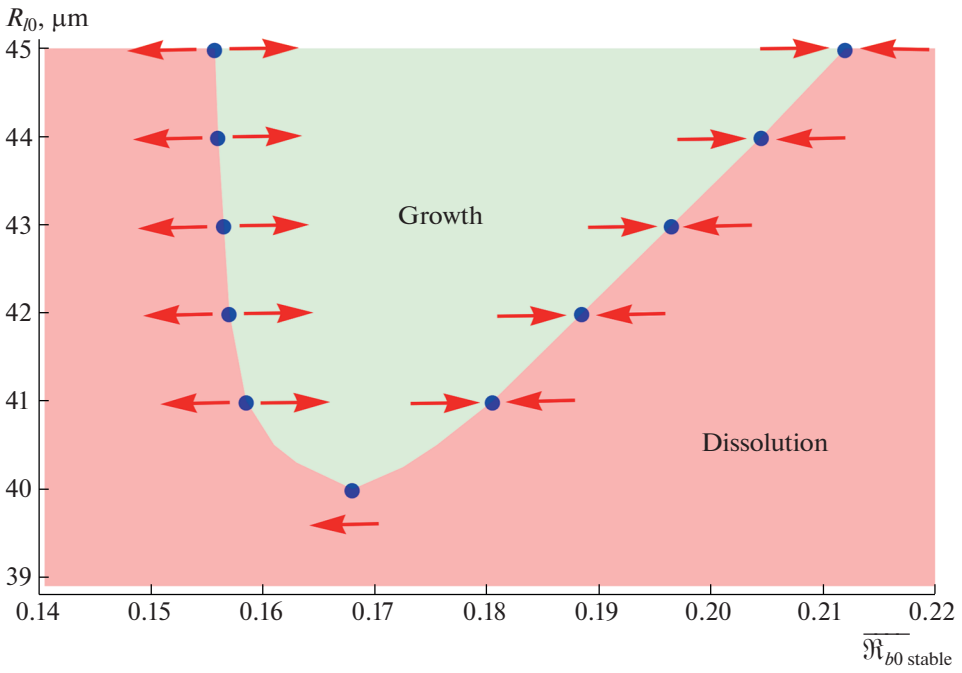

Fig. 4. The parameter space $\left(\overline{\Re_{b0}}, R_{l0}\right)$ for the fixed gas concentration 1.25% of c_{sp} (dashed line in Fig. 3).

The obtained results qualitatively like the results presented in [20], where the authors considered the mass transfer problem for the bubble oscillations under the external driving in a bulk compressible liquid (compare with Fig. 2(b) in this reference): at a small gas concentration a bubble totally dissolves in the liquid, whereas at a large gas concentration, exceeding the threshold one, a bubble has the attractor-like state, which provides a nonzero resulting stable bubble size. It should be mentioned that bubbles with radius $\Re_{b0}^{\circ} < \Re_{b0} < \Re_{b0}^{\mathrm{thres}}$ grow, whereas in [29] the authors showed that bubbles (nuclei) with the initial radius less than $\Re_{b0}^{\mathrm{thres}}$ dissolve regardless of the amount of the gas concentration in the liquid. In Fig. 3 the case of different liquid cell sizes is also presented in the range $R_{l0} = 30 \div 45$ μm. The analysis shows that the threshold bubble radius does not depend on the liquid cell size and equals $\Re_{b0}^{\mathrm{thres}} = 246$ nm, whereas the threshold gas concentration increases with the decrease of the liquid cell size, which is in line with the results in [29] (compare with Fig. 7(a) in this reference). It is expected that a following decrease of the liquid cell size will require a significant increase of the gas concentration for the formation of the threshold bubble size.

Figure 3 can also be presented in the parameter space $\left(\overline{\Re_{b0}}, R_{l0}\right)$ (see Fig. 4). For the fixed gas concentration 1.25% of c_{sp} we can consider the equilibrium diagram of the bubble behavior for different liquid cell sizes. Small values of R_{l0} result in the total dissolution of bubbles of any size, whereas at the critical value $R_{l0} = 40$ μm the stable bubble radius $\Re_{b0}^{\mathrm{thres}} = 246$ nm ($\overline{\Re_{b0}^{\mathrm{thres}}} \approx 0.17$) occurs. The diagram in Fig. 4 contains the growth (light shading) and dissolution (dark shading) regions, where the stable and unstable bubble states are indicated by the converging and diverging arrows, respectively. Here, the resulting stable bubble size monotonously increases with the increase of the liquid cell size, which is also accompanied by the expansion of the growth region. The similar approach was used in [20] to show the prerequisite for the stable bubble oscillations using the $(\Re_{b0}, \Delta p)$-parameter space (compare with Fig. 3 in this reference). It should be mentioned that the increase of the confinement size has a similar effect as an increase of the driving pressure amplitude in a bulk liquid resulting in the increase of the stable bubble size.

In Fig. 5a the case of different pressure amplitudes in the range $\Delta p = 390 \div 490$ kPa is presented for $R_{l0} = 40$ μm and $f_{\mathrm{ext}} = 70$ kHz. The analysis shows that in comparison with the variation of the liquid cell size (Fig. 3) the decrease of the pressure amplitude results in not only the increase of the threshold gas concentration, but also the formation of the larger the threshold bubble radius. This qualitatively agrees

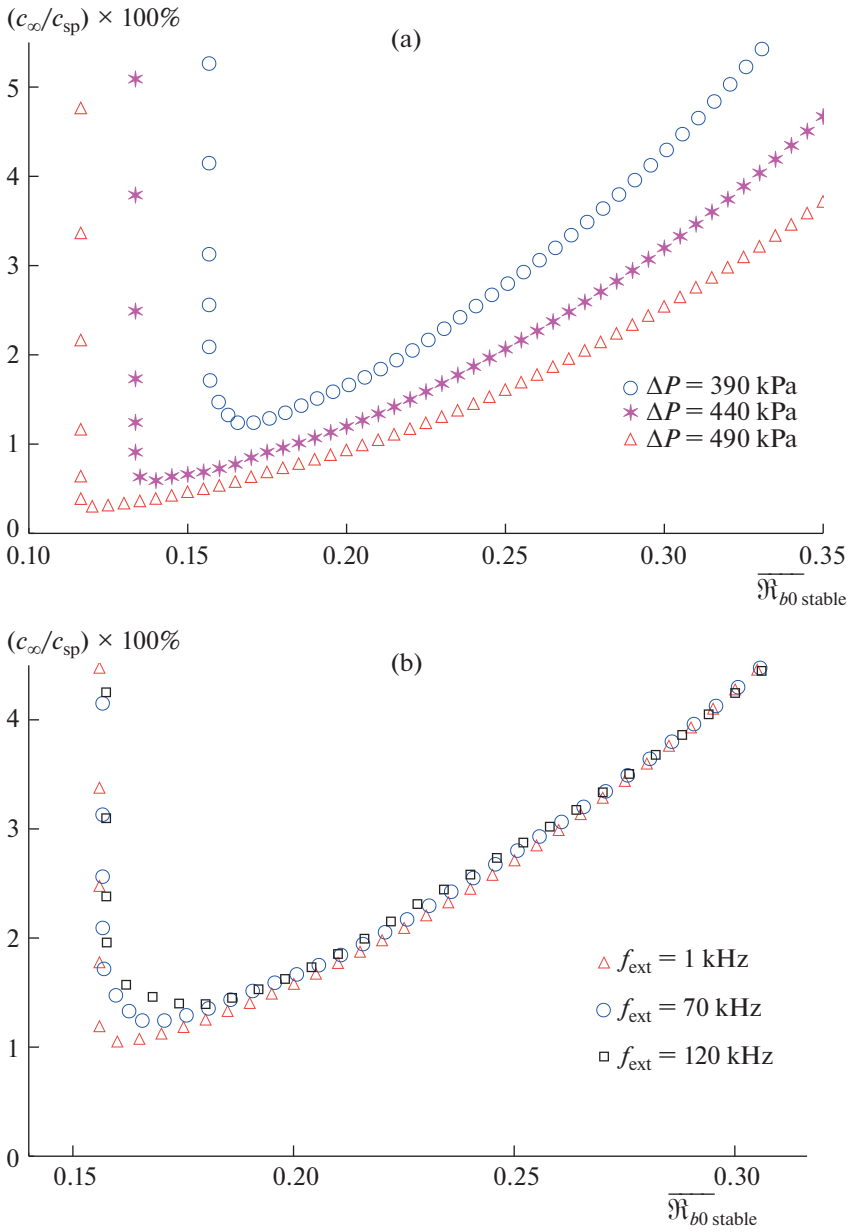

Fig. 5. The dependence of the gas concentration in the liquid cell on the resulting stable bubble size for different driving parameters: (a) the pressure amplitude in the range $\Delta p = 390 \div 490$ kPa, $R_{l0} = 40$ μm, $f_{ext} = 70$ kHz; (b) the frequency in the range $f_{ext} = 1 \div 120$ kHz, $R_{l0} = 40$ μm, $\Delta p = 390$ kPa.

with the results in [20], where the authors showed that the threshold gas concentration (and corresponding threshold bubble size) increases with the decrease of the driving pressure amplitude. In Fig. 5b the case of different frequencies of the external driving in the range $f_{ext} = 1 \div 120$ kHz is shown for $R_{l0} = 40$ μm and $\Delta p = 390$ kPa. For the gas concentration exceeding 3% of c_{sp} the dependence on the driving frequency is absent, and the resulting stable bubble forms with the same size. The insignificant difference occurs for the small gas concentration, such that the threshold gas concentration (also as the threshold bubble radius) tends to decrease with the decrease of the driving frequency.

3. DYNAMICS REGIMES OF A STABLE BUBBLE

In the previous section we show that the diffusion stability of the bubble provided by the two diffusion regimes (partial growth and partial dissolution). In the present section we consider an influence of the gas

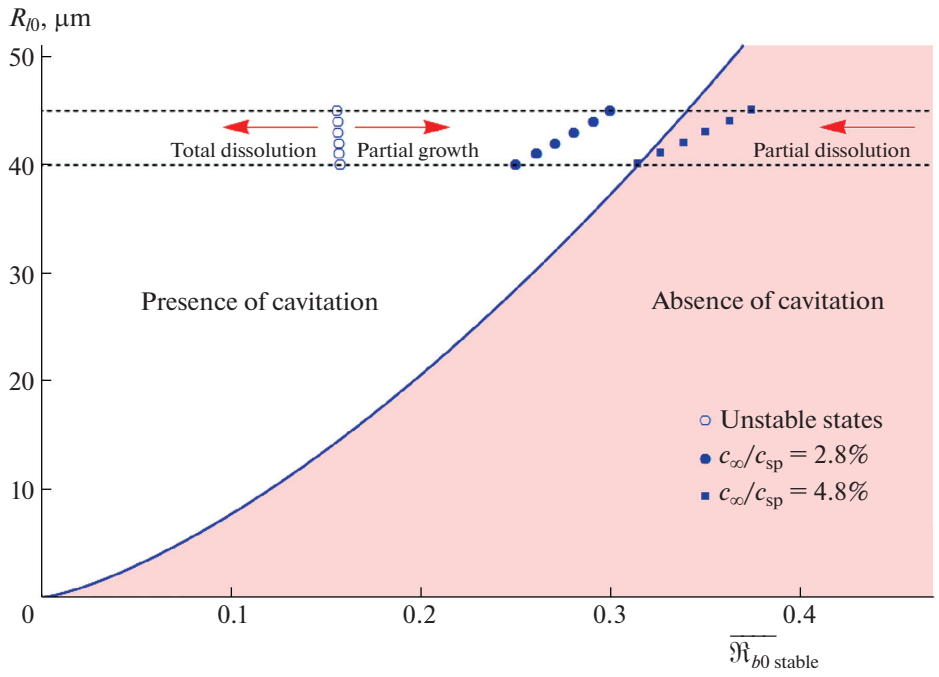

Fig. 6. The map of the dynamics regimes of the bubble and the equilibrium diagram of the bubble behavior for different gas concentrations in the liquid cell with a size of $R_{l0} = 40 \div 45$ μm. The solid line indicates the threshold bubble states, which provide the presence/absence of cavitation in the system at the fixed mass of gas in the bubble.

concentration in the liquid cell on transient bubble dynamics, which accompanies the formation of a stable bubble. In Fig. 6 the parameter space $\left(\overline{\Re}_{b0}, R_{l0}\right)$ is shown for the gas concentrations $c_\infty/c_{sp} = 2.8, 4.8\%$ and for the liquid cell size in the range $R_{l0} = 40 \div 45$ μm. Here, the equilibrium diagram qualitatively corresponds to the truncated dependence in Fig. 4, since at the given gas concentrations the threshold bubble radius forms at a smaller liquid cell size, which is out of the range $R_{l0} = 40 \div 45$ μm (see Fig. 3). The unstable states for both gas concentrations are almost the same and indicated by the open circles. The solid line is calculated using the approach developed in [28], where the fixed mass of gas in the bubble is assumed (see Eq. (27) in this reference). This line corresponds to the threshold bubble states, which divide the parameter space into two regions. In the first region, which is indicated as the "presence of cavitation," the bubble dynamics is characterized by both cavitation inception and cavitation vanishing as it is shown in Fig. 2b, whereas in the second region, the "absence of cavitation," the cavitation is completely suppressed by confinement and the bubble oscillations occur in a nonlinear (non-explosive) way, which is similar to the bubble behavior presented in [31] (Fig. 8b, dashed line).

The analysis shows that a bubble with a size of $\overline{\Re}_{b0} < 0.16$ will be subjected to the total dissolution for both gas concentrations. In this case, initial bubble dynamics is characterized by the cavitation phenomena, which include cavitation inception and cavitation vanishing. In [29] the authors showed that a decrease of the mass of gas in a bubble leads to an increase of the cavitation threshold and the pressure amplitude of the external driving becomes insufficient for cavitation inception, such that the bubble oscillates around its initial state in a nonlinear (non-explosive) way. After that, the surface tension enhances bubble dissolution due to the Henry's law, which results in the total bubble dissolution. The regime of the partial growth also realizes for both gas concentrations at $\overline{\Re}_{b0} > 0.16$ and limited by the stable bubble size for the corresponding liquid cell size and gas concentration in the liquid. In the case, when the gas concentration equals $c_\infty/c_{sp} = 2.8\%$, an increase of the mass of gas in the bubble does not noticeably change the bubble dynamics, which provides cavitation inception in the system. On the other hand, the bubble undergoes the partial dissolution when its size exceeds the stable bubble size for the corresponding liquid cell size as it is shown in Fig. 3. The region enclosed between the stable bubble sizes and the solid line ($0.24 < \overline{\Re}_{b0} < 0.30$) is also characterized by the bubble dynamics with cavitation inception. It should be

mentioned that the large bubbles $\overline{\Re_{b0}} > 0.30$ oscillate without cavitation inception. As a result, during the regime of the partial dissolution transient bubble dynamics realizes such that starting from the relatively small nonlinear oscillations a decrease of the mass of gas in a bubble intensifies a bubble response and cavitation initiates at intersection of the solid line in Fig. 6.

Another case of transient bubble dynamics is presented in Fig. 6 for the gas concentration $c_\infty/c_{sp} = 4.8\%$. Here, the diffusion stability is provided by the bubble dynamics in the absence of cavitation. In this case, the partial dissolution is accompanied by the nonlinear bubble dynamics with no abrupt cavitation bubble growth. However, in the regime of the partial growth the bubble initially undergoes cavitation inception, which continuously damps and vanishes at intersection of the solid line.

Thus, the gas concentration in confined liquid has a significant influence on the bubble dynamics, which accompanies the diffusion regimes in the bubble-in-cell system. At the fixed gas concentration the diffusion regimes, which provide the diffusion stability (partial growth and partial dissolution), can be formed under the condition of the three dynamic regimes of the bubble: 1) in the presence of cavitation inception, 2) in the absence of cavitation, and 3) direct or reverse combination of the previous two dynamic regimes. As a result, the gas concentration plays a role of the governing parameter, which allows to choose a certain dynamics regime during the formation of a stable bubble size.

4. POTENTIAL APPLICATIONS

Based on the theoretical findings obtained in the present study we hypothesize that the diffusion and bubble dynamics regimes in confined liquid may offer potential for further study and use in industrial-scale applications of ultrasound. The possible applications are briefly discussed below.

• The drug delivery

The transient bubble dynamics resembles a resonance-like bubble behavior, where the multiple increase in bubble radius is observed at reaching of a certain bubble size due to the rectified diffusion at the fixed driving frequency. In this case, the bubble expansion in confined liquid is limited by a finite size, which allows to control bubble dynamics in comparison with explosive bubble growth at real bubble resonance. Such bubble behavior has a potential to be considered in the study of the drug delivery developing mitigation strategies for bubble collapse in vasculature with the following disrupting of a stabilizing shell and releasing of therapeutic payload. The transient bubble dynamics can also be helpful to initiate chemical and physical processes, and for increasing rates of chemical reactions by the mass transfer effects.

• The degassing of epoxy resin during the manufacturing of composite materials

Gaseous components dissolved in the resin at room conditions are a key source of bubbles once resin pressure is reduced to below atmospheric pressure. This mechanism of bubble formation is of interest during the manufacturing of composite materials via Vacuum Assisted Resin Infusion (VARI), with the infusion and post-filling stages being completed significantly below atmospheric pressure [33]. The presence of the bubbles in this process may crucially degrade the mechanical properties of composite materials. To prevent bubble formation, the standard degassing procedure is used, where the resin samples are placed into a vacuum chamber and the pressure decreased to the specified level. However, air bubbles can be still entrapped during the impregnation stage due to differences in intra-tow and inter-tow resin velocities. Some manufacturers prefer to heat the resin during infusion as this may help the resin to flow by reducing the viscosity, which also reduces the curing time [34]. On the other hand, the resin viscosity may gradually increase owing to curing, especially in places with flow stagnation, which can occur in large-sized composite structures with complex geometry [35]. As a result, during (post-)filling stage, when resin is partially cured, bubbles can be effectively trapped in temporary confinement of fluidic resin inclusions within the composite specimen. In this case, acoustic radiation can be potentially applied to resin on-site to dissolve bubbles under certain conditions providing the regime of the total bubble dissolution.

• The bubble dissolution in the ink channel

Another example is the drop-on-demand piezo-acoustic inkjet printing, where the typical control and design parameters include the driving frequency in the range of 10–100 kHz, the nozzle pressure exceeding 150 kPa to allow for jetting at the required velocities, the size of the nozzle with a diameter and length around 20–30 μm, a droplet diameter around 20 μm, and others [14]. Considering the proximity of the scales of the control parameters in the inkjet printing technology and in the present study, we hypothesize that the diffusion regimes can be potentially realized at certain auxiliary conditions, which are the slightly changed control parameters of the main driving. The similar hypothesis was proposed in [14], where the author mentioned that to optimize inkjet printing process it is necessary to find ways either to avoid air

entrainment or to get rid of the bubble faster than its passive dissolving, e.g., by applying some kind of recovery pulse to the piezo actuator in an early phase after bubble entrainment.

SUMMARY

In this study, the diffusion stability of the oscillating spherical bubble in the compressible spherical liquid cell surrounded by the infinite elastic solid medium is considered. We assume that the liquid has some amount of dissolved gas, which is involved in the mass transport by the periodic time-dependent pressure in the solid far away from the liquid cell, providing the specific driving to the system.

The work is based on the engineering approximation according to which the bubble growth/reduction is considered on average, such that during the period of the external driving the mass of gas in the bubble does not noticeably change. The governing equation is derived assuming that the mean mass flux in the bubble equals to zero, and the bubble size keeps constant during the volume oscillations on average. It allows to consider the equilibrium diagram of the diffusion stability of the bubble in confined liquid under external driving force. Three possible diffusion regimes are revealed: 1) total bubble dissolution, 2) partial bubble dissolution, and 3) partial bubble growth, where the last two regimes correspond to the diffusion stability in the bubble-in-cell system. The analysis shows that the regimes of the partial dissolution and partial growth can be formed under the condition of the three dynamic regimes of the bubble: 1) in the presence of cavitation inception, where both cavitation inception and cavitation vanishing are realized; 2) in the absence of cavitation, where cavitation is completely suppressed by confinement and the bubble oscillations occur in a nonlinear (non-explosive) way, and 3) combination of the previous two dynamic regimes, which corresponds to transient bubble dynamics with activation/deactivation of cavitation inception. In this case, concentration of dissolved gas in the liquid plays a role of the governing parameter, which allows to control a dynamics regime during the formation of a stable bubble size. The influence of the gas concentration in the liquid cell on the resulting stable bubble size is considered for different liquid cell sizes, pressure amplitudes, and frequencies of the external driving. The obtained results are compared with the results for the case of the stable bubble oscillations in the pressure sound field in a bulk liquid.

This work provides a theoretical framework to develop ultrasound technologies associated with the mass transfer applications for bubbles in confined systems, as well as for validation of the more complex numerical models and codes.

FUNDING

This work was supported by ongoing institutional funding. No additional grants to carry out or direct this particular research were obtained.

CONFLICT OF INTEREST

The authors of this work declare that they have no conflicts of interest.

REFERENCES

1. Clift, R., Grace, J., and Weber, M., *Bubbles, Drops and Particles,* New York: Academic, 1978.
2. Gondrexon, N., Renaudin, V., Boldo, P., Gonthier, Y., Bernis, A., and Pettier, C., Degassing effect and gas-liquid transfer in a high frequency sonochemical reactor, *J. Chem. Eng.*, 1997, vol. 66 (1), pp. 21–26. https://doi.org/10.1016/S1385-8947(96)03124-5
3. Kim, W., Kim, T.-H., Choi, J., and Kim, H.-Y., Mechanism of particle removal by megasonic waves, *Appl. Phys. Lett.*, 2009, vol. 94 (8), p. 081908. https://doi.org/10.1063/1.3089820
4. Lauterborn, W. and Kurz, T., Physics of bubble oscillations, *Rep. Prog. Phys.*, 2010, vol. 73, p. 106501. https://doi.org/10.1088/0034-4885/73/10/106501
5. Crum, L.A., Mason, T.J., Reisse, J.L., and Suslick, K.S., *Sonochemistry and Sonoluminescence,* Dordrecht: Springer, 1999. https://doi.org/10.1007/978-94-015-9215-4
6. Wang, S.S., Jiao, Z.J., Huang, X.Y., Yang, C., and Nguyen, N.T., Acoustically induced bubbles in a microfluidic channel for mixing enhancement, *Microfluid Nanofluidics,* 2009, vol. 6, pp. 847–852. https://doi.org/10.1007/s10404-008-0357-6

7. Avvaru, B., Venkateswaran, N., Uppara, P., Iyengar, S.B., and Katti, S.S., Current knowledge and potential applications of cavitation technologies for the petroleum industry, *Ultrason. Sonochem.*, 2018, vol. 42, pp. 493–507. https://doi.org/10.1016/j.ultsonch.2017.12.010
8. Batchelor, D.V.B., Armistead, F.J., Ingram, N., Peyman, S.A., McLaughlan, J.R., Coletta, P.L., and Evans, S.D., The influence of nanobubble size and stability on ultrasound enhanced drug delivery, *Langmuir*, 2022, vol. 38, pp. 13943–13954. https://doi.org/10.1021/acs.langmuir.2c02303
9. Marmottant, P. and Hilgenfeldt, S., Controlled vesicle deformation and lysis by single oscillating bubbles, *Nature,* 2003, vol. 423, pp. 153–156. https://doi.org/10.1038/nature01613
10. Coussios, C.C. and Roy, R.A., Applications of acoustics and cavitation to noninvasive therapy and drug delivery, *Annu. Rev. Fluid Mech.*, 2008, vol. 40, pp. 395–420. https://doi.org/10.1146/annurev.fluid.40.111406.102116
11. Stride, E. and Coussios, C., Nucleation, mapping and control of cavitation for drug delivery, *Nat. Rev. Phys.*, 2019, vol. 1, pp. 495–509. https://doi.org/10.1038/s42254-019-0074-y
12. Moreno Soto, Á., Lohse, D., and Van der Meer, D., Diffusive growth of successive bubbles in confinement, *J. Fluid Mech.*, 2020, vol. 882, p. A6. https://doi.org/10.1017/jfm.2019.806
13. Hsieh, D. and Plesset, M.S., Theory of rectified diffusion of mass into gas bubbles, *J. Acoust. Soc. Am.*, 1961, vol. 33, pp. 206–215. https://doi.org/10.1121/1.1908621
14. Lohse, D., Fundamental fluid dynamics challenges in inkjet printing, *Annu. Rev. Fluid Mech.*, 2022, vol. 54, pp. 349–382. https://doi.org/10.1146/annurev-fluid-022321-114001
15. Reinten, H., Jethani, Y., Fraters, A., Jeurissen, R., Lohse, D., Versluis, M., and Segers, T., Resonance behavior of a compliant piezo-driven inkjet channel with an entrained microbubble, *J. Acoust. Soc. Am.*, 2022, vol. 151, pp. 2545–2557. https://doi.org/10.1121/10.0009784
16. Fraters, A., van den Berg, M., de Loore, Y., Reinten, H., Wijshoff, H., Lohse, D., Versluis, M., and Segers, T., Inkjet nozzle failure by heterogeneous nucleation: Bubble entrainment, cavitation, and diffusive growth, *Phys. Rev. Appl.*, 2019, vol. 12, p. 064019. https://doi.org/10.1103/PhysRevApplied.12.064019
17. Eller, A. and Flynn, H.G., Rectified diffusion during nonlinear pulsations of cavitation bubbles, *J. Acoust. Soc. Am.*, 1965, vol. 37, pp. 493–503. https://doi.org/10.1121/1.1909357
18. Fyrillas, M.M. and Szeri, A.J., Dissolution or growth of soluble spherical oscillating bubbles, *J. Fluid Mech.*, 1994, vol. 277, pp. 381–407. https://doi.org/10.1017/S0022112094002806
19. Brenner, M.P., Lohse, D., Oxtoby, D., and Dupont, T.F., Mechanisms for stable single bubble sonoluminescence, *Phys. Rev. Lett.*, 1996., vol. 76, pp. 1158–1161. https://doi.org/10.1103/PhysRevLett.76.1158
20. Akhatov, I., Gumerov, N., Ohl, C.D., Parlitz, U., and Lauterborn, W., The role of surface tension in stable single-bubble sonoluminescence, *Phys. Rev. Lett.*, 1997, vol. 78, pp. 227–230. https://doi.org/10.1103/PhysRevLett.78.227
21. Hilgenfeldt, S., Brenner, M.P., Grossmann, S., and Lohse, D., Analysis of Rayleigh–Plesset dynamics for sonoluminescing bubbles, *J. Fluid Mech.*, 1998, vol. 365, pp. 171–204. https://doi.org/10.1017/S0022112098001207
22. Brenner, M.P., Hilgenfeldt, S., and Lohse, D., Single-bubble sonoluminescence, *Rev. Mod. Phys.*, 2002, vol. 74, pp. 425–484. https://doi.org/10.1103/RevModPhys.74.425
23. Church, C.C., The effects of an elastic solid surface layer on the radial pulsations of gas bubbles, *J. Acoust. Soc. Am.*, 1995, vol. 97, pp. 1510–1521. https://doi.org/10.1121/1.412091
24. Obreschkow, D., Kobel, P., Dorsaz, N., de Bosset, A., Nicollier, C., and Farhat, M., Cavitation bubble dynamics inside liquid drops in microgravity, *Phys. Rev. Lett.*, 2006, vol. 97, pp. 094502. https://doi.org/10.1103/PhysRevLett.97.094502
25. Fourest, T., Laurens, J.M., Deletombe, E., Dupas, J., and Arrigoni, M., Confined Rayleigh-Plesset equation for hydrodynamic ram analysis in thin-walled containers under ballistic impacts, *Thin-Walled Struct.*, 2015, vol. 86, pp. 67–72. https://doi.org/10.1016/j.tws.2014.10.003

26. Vincent, O. and Marmottant, P., On the statics and dynamics of fully confined bubbles, *J. Fluid Mech*., 2017, vol. 827, pp. 194–224.
https://doi.org/10.1017/jfm.2017.487
27. Wang, Q.X., Oscillation of a bubble in a liquid confined in an elastic solid, *Phys. Fluids,* 2017, vol. 29, p. 072101.
https://doi.org/10.1063/1.4990837
28. Leonov, K. and Akhatov, I., Dynamics of an externally driven cavitation bubble in an elastic microconfinement, *Phys. Rev. E.*, 2021, vol. 104, p. 015105.
https://doi.org/10.1103/PhysRevE.104.015105
29. Leonov, K. and Akhatov, I., The influence of dissolved gas on dynamics of a cavitation bubble in an elastic micro-confinement, *J. Heat Mass Transf. Res*., 2022, vol. 196, p. 123295.
https://doi.org/10.1016/j.ijheatmasstransfer.2022.123295
30. Doinikov, A.A. and Marmottant, P., Natural oscillations of a gas bubble in a liquid-filled cavity located in a viscoelastic medium, *J. Sound Vibr*., 2018, vol. 420, pp. 61–72.
https://doi.org/10.1016/j.jsv.2018.01.034
31. Leonov, K. and Akhatov, I., Towards a theory of dynamics of a single cavitation bubble in a rigid micro-confinement, *Int. J. Multiph. Flow,* 2020, vol. 130, p. 103369.
https://doi.org/10.1016/j.ijmultiphaseflow.2020.103369
32. Brennen, C.E., *Cavitation and Bubble Dynamics,* New York: Cambridge University Press, 2013.
https://doi.org/10.1017/CBO9781107338760
33. Van Oosterom, S., Schreier, A., Battley, M., Bickerton, S., and Allen, T., Influence of dissolved gasses in epoxy resin on resin infusion part quality, *Compos. Part A Appl. Sci. Manuf.*, 2020, vol. 132, p. 105818.
https://doi.org/10.1016/j.compositesa.2020.105818
34. Afendi, Md, Banks, W.M., and Kirkwood, D., Bubble free resin for infusion process, *Compos. Part A Appl. Sci. Manuf*., 2005, vol. 36 (6), pp. 739–746.
https://doi.org/10.1016/j.compositesa.2004.10.030
35. Shevtsov, S., Zhilyaev, I., Chang, S-H., Wu, J-K., Huang, J-P., and Snezhina, N., Experimental and numerical study of vacuum resin infusion for thin-walled composite parts, *Appl. Sci*., 2020, vol. 10 (4), p. 1485.
https://doi.org/10.3390/app10041485

Translated by the authors